



Research Paper

Vacuum heat treatments of titanium porous structures

Shaaz Ghouse^a, Reece N. Oosterbeek^a, Aisha Tayub Mehmood^a, Filippo Vecchiato^b,
David Dye^b, Jonathan R.T. Jeffers^{a,*}

^a Department of Mechanical Engineering, Imperial College London, London SW7 2AZ, United Kingdom

^b Department of Materials, Imperial College London, London SW7 2AZ, United Kingdom

ARTICLE INFO

Keywords:

Porous Material
Fatigue
Titanium
Heat Treatment

ABSTRACT

Additive manufacturing (AM) of Ti-6Al-4V enables rapid fabrication of complex parts, including porous lattices which are of interest for aerospace, automotive, or biomedical applications, however currently the fatigue resistance of these materials is a critical limitation. Engineering the alloy microstructure provides a promising method for increasing fatigue strength, but conventional heat treatment procedures are known to produce atypical results for AM and porous samples, and must therefore be optimised for these materials. Using vacuum heat treatment, microstructures comparable to those observed for conventional wrought and heat treated alloys were achieved with porous AM Ti-6Al-4V. Fine lamellar microstructures were produced using sub-transus heat treatment at 920 °C, while coarse lamellar microstructures were produced using super-transus heat treatment at 1050 °C or 1200 °C. Increasing the heat treatment temperature increased the elastic modulus from 2552 ± 22 MPa to a maximum of 2968 ± 45 MPa, due to strut sintering increasing the effective strut thickness, and removal of prior β -grain orientation. Heat treatment eliminated the brittle α' martensite phase in favour of an $\alpha + \beta$ mixture, where the phase boundaries and β -phase provide greater resistance to crack propagation. Super-transus heat treatments increased the α -lath size which typically reduces crack propagation resistance, however strut sintering reduced surface crack initiation sites, increasing the fatigue strength by 75% from 4.86 MPa for the as-built material to a maximum of 8.51 MPa after 1200 °C heat treatment. This work demonstrates that vacuum heat treatment is effective at tuning the micro- and macro-structure of porous AM Ti-6Al-4V, thereby improving the crucial fatigue resistance.

1. Introduction

Additive manufacturing (AM) of titanium alloys is an ascendant technique, providing the ability to rapidly fabricate complex parts, with reduced wastage and machining time through near net shape manufacturing [1]. A particular advantage is the ability to fabricate porous lattice structures, which are challenging to produce through conventional processing methods, but have a wide array of benefits. In aerospace or automotive applications, AM porous structures allow lightweight design, alongside topological optimisation to design lightweight parts specific to their stress trajectories [2,3]. In biomedical applications, AM biocompatible porous Ti-6Al-4V is especially promising for orthopaedic implants, where the high degree of control allows the elastic modulus to be tailored to match that of bone at both the bulk and local level, reducing the effects of stress shielding and promoting bone ingrowth [4–7].

In these applications, the fatigue behaviour of the material and lattice structure is of crucial importance due to the high cyclic loads experienced. Under compressive fatigue testing, AM lattices, like other porous metals, display three-stage strain accumulation behaviour involving initial plastic strain followed by a period where strain is nearly constant until eventual failure and rapid strain increase [8]. Recent work has demonstrated that the topological design of the lattice (unit cell, porosity) can have an impact on this fatigue behaviour, however in contrast to the quasi-static mechanical properties, the topology effect is less important than the material type and manufacturing defects for fatigue performance [9].

Despite over 60 years of research there remains conflicting evidence on the optimal microstructure of wrought Ti-6Al-4V for maximising high cycle fatigue (HCF) strength. This is likely due to variations in thermo-mechanical history within these microstructural forms (which in turn affect the grain size and phase composition), as well as experimental and

* Corresponding author.

E-mail address: j.jeffers@imperial.ac.uk (J.R.T. Jeffers).

<https://doi.org/10.1016/j.addma.2021.102262>

Received 2 April 2021; Received in revised form 18 August 2021; Accepted 18 August 2021

Available online 20 August 2021

2214-8604/© 2021 The Authors. Published by Elsevier B.V. This is an open access article under the CC BY license (<http://creativecommons.org/licenses/by/4.0/>).

reproducibility limitations inherent to standard fatigue testing methods. Wu et al. [10] reviewed literature from 1972 to 2013 to systematically assess the microstructural parameters affecting HCF, concluding that microstructure plays a key role in the fatigue properties of wrought Ti-6Al-4V, and that fatigue strength increases in the order of equiaxed, lamellar and bimodal microstructures. The findings of Fan et al. [11] contradict this, where fatigue strength was seen to increase in the order of α' -martensite, Widmanstätten, bimodal, and equiaxed microstructures. Several other studies also demonstrate contradictory results [12–15], thus it is clear that further work is needed to separate the effect of microstructural form from the compounding effects of grain and crack size, surface finish, phase composition, and other experimental parameters.

This is further complicated by the use of AM to produce porous titanium alloy lattices, which often behave differently in fatigue to their solid monolithic counterparts because of their high surface area characterised by surface defects, namely semi-fused particles and cracks. Fatigue strength is strongly influenced by two factors: crack initiation and crack propagation, i.e. the resistance to a crack opening and how fast that crack will spread through the material leading to failure. For samples with few defects, resistance to fatigue crack initiation is more advantageous than resistance to crack propagation, however the defect-rich nature of the surface of AM parts makes resistance to crack initiation difficult.

Post-processing surface treatments such as shot peening, milling, chemical, and electrochemical methods can reduce the effect of these defects and provide superior fatigue performance [16–18], although these techniques are challenging to implement with a porous structure and can still leave cracks and surface imperfections on struts and at nodes. As there is difficulty in eliminating all surface defects or imperfections in porous materials, tuning the microstructure to improve crack propagation resistance is essential for applications that require maximal high-cycle fatigue strength. Therefore the focus on microstructure optimisation should be on resistance to crack propagation - without a reliable method to achieve an ideal surface finish, microstructure alterations can be used to improve fatigue life.

Ti-6Al-4V produced using PBF (Powder bed fusion) typically has a martensitic α' microstructure as a result of the fast cooling rates experienced, which has notoriously poor fatigue properties [19–21]. Well-established heat treatment procedures developed for conventional wrought parts allow transformation of the α' martensite to an $\alpha + \beta$ mixture, improving fatigue properties, however these show different results for AM parts due to their thermal history and must therefore be adapted and optimised to achieve the desired microstructure and properties [22,23]. During heat treatment it is not only the heating and cooling steps that can affect the subsequent properties, but also the atmosphere used. Argon is often used as an inert atmosphere during building, heat treatment, and high-pressure heat treatment (HIP: hot isostatic pressing), however impurities in the gas can alter the microstructure and embrittle the material [24]. Titanium alloys are particularly vulnerable to hydrogen pickup leading to significant embrittlement, however hydrogen content can be reduced by vacuum heat treatment [25,26].

Despite the potential of porous Ti-6Al-4V and the importance of its fatigue properties, very little research has focused on heat treatment of these materials to alter the microstructure and improve the fatigue strength. Brenne et al. investigated vacuum heat treatment of cellular sandwich structures and conducted limited fatigue testing, finding that coarsening of the α phase and formation of β phase extended the fatigue life significantly [27]. Wauthle et al. found that HIP treatment transforms the as-built α' martensitic phase to lamellar $\alpha + \beta$, reducing the strength but increasing ductility, which was predicted to be advantageous for fatigue life [28]. In this work we investigate the effect of different vacuum heat treatments on the microstructure of PBF porous Ti-6Al-4V, and comprehensively characterise the resulting quasi-static mechanical and high cycle fatigue properties.

2. Material and methods

2.1. Porous sample design

The porous structure used in this study was designed in Rhinoceros 5.0 (Robert McNeel & Associates) using a method detailed previously [29]. This method is explained briefly here and illustrated in Fig. 1. A random distribution of points, generated via a Poisson Disk algorithm, filled a $\phi 13$ mm x 21 mm cylindrical volume. These points represented the nodes of the stochastic porous structure. The nodes were then joined by zero thickness lines with a specified connectivity [30]. Struts with a build angle of less than 30° were removed from the structure. The macro dimensions of the designed structure ensured a Height:Diameter ratio of > 1.5 and conformity to ISO 13314:2011 after removal from the build plate [31]. The software platform Material Engine 1.0 (Betatype Ltd.) was used to generate the slice data and assign laser parameters (build file) directly from the CAD data. Solid specimens were also designed, with dimensions $\phi 10$ mm x 15 mm, in order to compare their microstructure development to their porous counterparts.

2.2. Materials and manufacturing

All specimens in this study were fabricated using an AM250 metal powder bed fusion (PBF) system (Renishaw plc., UK). This procedure has been described in detail elsewhere [30]. Samples were manufactured in medical grade titanium (Grade 23 alloy Ti-6Al-4V ELI [32] hereafter referred to as Ti64). Spherical Ti64 powder was supplied by Carpenter Additive (Carpenter Technology Corp., USA), with a particle size range of 10–45 μm and D_{50} value of 27 μm . A contour scanning strategy was used, with 70 μm contour diameter, 50 W laser power, 50 μm point distance, 600 μs exposure time, and 50 μm layer thickness. Samples were built onto a titanium build plate, and removed after fabrication by wire-cut electrical discharge machining, after which they were ground to ensure the top and bottom surfaces were parallel, and ultrasonically cleaned in ethanol. In total 104 specimens were manufactured, including 100 lattice specimens and 4 solid specimens. In total 72 specimens were used for fatigue testing, 20 for relative density measurements, 4 for micro-CT measurement, and 4 for chemical analysis.

2.3. Vacuum heat treatment

Samples were divided into 4 groups, with each group containing 25 porous specimens and 1 solid specimen. One group remained in the as-built condition and was not subject to any thermal heat treatments. The remaining 3 groups were each heat treated as follows. In a vacuum furnace (Specnow VF1218H), samples were heated to the desired temperature (920 $^\circ\text{C}$, 1050 $^\circ\text{C}$ or 1200 $^\circ\text{C}$) under vacuum (10^{-5} mbar) at a rate of 8 $^\circ\text{C}/\text{min}$; temperatures were chosen to provide both sub-transus and super-transus heat treatments, to investigate the effect of β -grain formation during heat treatment upon the resulting microstructure and mechanical properties. Further temperature elevation also allows the effects of changes in lattice macro-morphology (i.e. sintering etc.) to be identified. Samples were held for two hours at temperature and then furnace cooled to room temperature under vacuum.

2.4. Quasi static testing

Quasi-static mechanical testing was carried out in compression configuration, according to ISO 13314:2011 [31]. A servo-hydraulic materials testing machine (Instron 8872) was used, with 5, 10, or 25 kN load cells depending on the sample. Spherically seated, lubricated, and hardened (>62 HRC) compression platens were used, with the sample centred between upper and lower platens. A constant strain rate of 2 mm/min was used (~ 0.1 strain/min). Displacement was measured using two LVDTs (RDP D6/05000A, RDP Electronics Ltd., UK) with a sampling rate of 30 Hz. Strain was calculated from the average

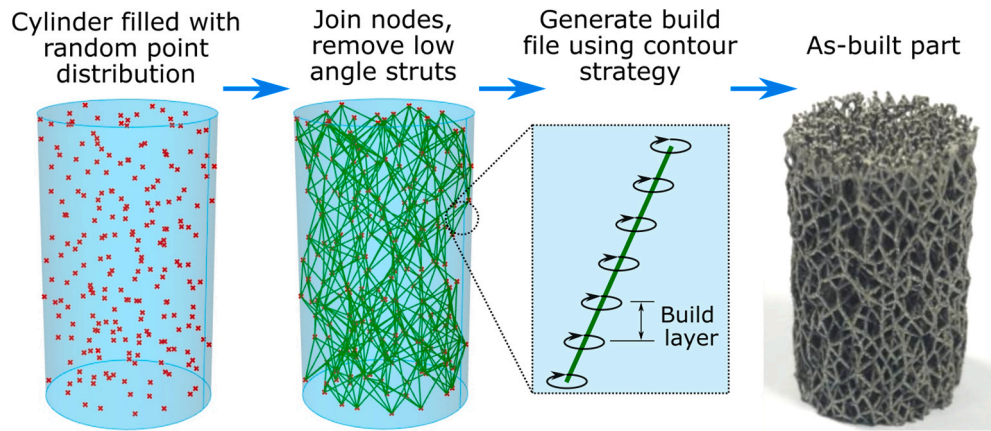


Fig. 1. Workflow for design and fabrication of stochastic porous strut-based lattices. Points and struts in diagrams are simplified for clarity and are not to scale.

LVDT displacements and the initial height of the sample, and stress was calculated using the measured load and initial sample cross-sectional area.

For each unique sample a preliminary test was carried out up to 50% compressive strain to gather an estimate of the yield strength. A further 5 samples (for each set of conditions) were then tested to evaluate the mechanical properties, by loading samples up to 50% compressive strain, with a hysteresis loop between 70% and 20% of the estimated yield strength. This removes the effect of local plastic deformation that occurs in porous structures and reduces the initial loading slope, allowing more accurate measurement of the elastic modulus. The elastic modulus (E) was calculated by linear regression of the hysteresis loop, and the yield strength (σ_y) was taken at a 1.0% compressive strain offset from the elastic modulus. The yield strength and UTS described in this work are all taken from the initial stress peak at around 5% strain, before the plateau stress during compressive flow.

2.5. Fatigue testing

Fatigue testing was also carried out in compression-compression configuration, according to ISO 1099:2017 [33], using a similar setup as for the quasi-static testing above with some modifications. A 0.25, 1, or 5 kN load cell was used depending on the sample, and displacement was measured using a single un-guided LVDT (RDP D6/05000URA, RDP Electronics Ltd., UK). Fatigue testing was carried out under load control using a 15 Hz sinusoidal waveform, with $R = 0.1$ (min:max stress ratio). Tests were carried out until 10^6 cycles were reached or until catastrophic failure, defined based on previous work as 5% strain, to allow adequate examination of failure planes.

To generate an S - N curve, two specimens were tested each at 5 different stress levels (80%, 66.7%, 53.3%, 40% & 30% of the yield stress) and consequently the staircase method was used to determine the average fatigue strength at 10^6 cycles according to ISO 12107:2003 [34]. For the staircase method, initial test stresses were chosen based on values from the literature, and the step size was set at 1.25% of the yield strength.

2.6. Morphological and chemical analysis

The overall relative density of the structure for each unique specimen was measured by weighing the samples under atmospheric conditions ($n = 5$). Relative density was calculated using the actual weight, and the theoretical weight of the macro-scale cylindrical volume using a density of 4.42 g/cm^3 for Ti64. This was validated using micro-CT (Bruker Skyscan 1172), to measure internal porosity (pores in struts) and measure strut and pore size. A single porous specimen per heat treatment was scanned over a height of 5 mm with a $5 \mu\text{m}$ resolution. CT images

were reconstructed and then analysed in CTAn 1.16.4.1 (Bruker microCT N.V.).

To examine the microstructure, a single porous and solid sample per heat treatment condition was sectioned both parallel and perpendicular to the build direction, mounted, ground with SiC papers (400, 800, 1200 and 2400 grit) and polished with diamond suspensions (6 and $1 \mu\text{m}$) and a colloidal silica suspension ($0.04 \mu\text{m}$), and etched with Kroll's reagent. After microstructure analysis, the mounted solid specimens were re-polished and underwent electron backscatter diffraction (EBSD). EBSD was performed with a Bruker e-Flash FS EBSD detector on a Zeiss Gemini Sigma 300 FEG SEM. Imaging was done at $\sim 20 \text{ mm}$ working distance at 500x magnification, 20 kV accelerating voltage, with an EBSD map size of 400×300 pixels and a pixel resolution of $0.8\text{--}1 \mu\text{m}$.

Oxygen, nitrogen and hydrogen levels were determined on a single porous specimen for each thermal treatment condition by Carpenter Additive Ltd. The levels were measured using an automated LECO ONH836 with inert gas fusion infrared and thermal conductivity detection. O and N were determined by ASTM E-1019 whilst H was determined by ASTM E-1447. Samples of 0.15–0.30 g were cut from the porous specimen, cleaned, and loaded into a graphite crucible (LECO 782–720). The instrument blank was measured using empty crucibles, and calibration was carried out using standards with known O, N and H content. After blanking and calibration, samples were measured using the automated inert gas fusion analyser (LECO ONH836), which heats the sample to release gases and convert them (O to CO and CO_2 , H to H_2O) for subsequent detection by infrared (CO, CO_2 , H_2O) and thermal conductivity (N_2) detectors. The test accuracy depends on the analyte content; but for titanium the limit of detection is 50 ppm for oxygen, 10 ppm for nitrogen, and 0.5 ppm for hydrogen.

3. Results

Typical quasi-static stress-strain curves for the four different thermal conditions are seen in Fig. 2. Regardless of heat treatment, all structures display a local maximum followed by a brittle failure and brittle collapse throughout the plateau region. The as-built, 1050°C and 1200°C structures all appear to have similar strain at maximum stress and strain at failure, whilst the samples subjected to the 920°C heat treatment may be slightly more ductile. The yield and maximum strength of the structures remained relatively constant between the different heat treatment conditions ranging from ~ 32 to 35 MPa (Table 1). The elastic modulus increased with increasing heat treatment holding temperature, with modulus increasing from $2.56 \pm 0.02 \text{ GPa}$ for the as-built samples to $2.97 \pm 0.04 \text{ GPa}$ for the 1200°C specimens (Table 1).

For all specimens, angled crush bands (fracture planes) were observed (Fig. 3), which is characteristic of compressive failure in both stochastic porous materials and brittle continuum materials. These are

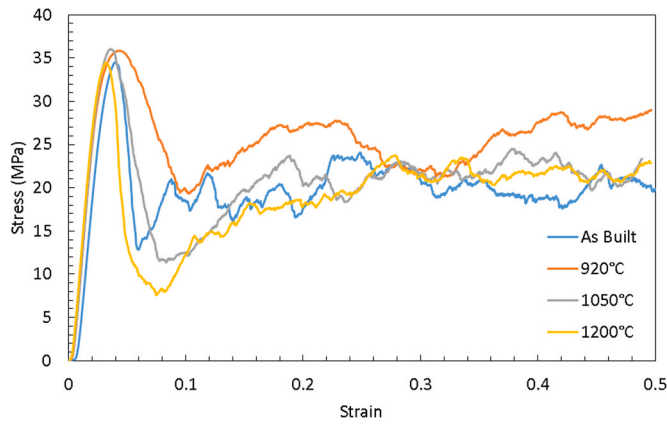


Fig. 2. Representative stress-strain curves for compression testing of AM Ti64 stochastic lattices, in as-built condition and after vacuum heat treatment at 920, 1050, and 1200 °C.

Table 1

Morphological, mechanical and chemical properties of Ti64 porous materials with varying heat treatments.

	Heat Treatment Condition			
	As-built	920 °C	1050 °C	1200 °C
Relative Density (%)	15.57	15.64	15.7	15.41
Internal Porosity (%)	0.0034	0.0040	0.0040	0.0033
Mean Strut Thickness (um)	225.45	224.67	224.32	223.79
Mean Pore Size (um)	753.5	747.41	750.58	760.04
E (MPa)	2552 ± 22	2726 ± 42	2921 ± 48	2968 ± 45
σ_y (MPa)	34.8 ± 0.3	32.8 ± 0.4	34.6 ± 0.5	33.3 ± 0.3
UTS (MPa)	34.9 ± 0.3	33.4 ± 0.5	34.7 ± 0.5	33.6 ± 0.5
σ_f at 10^6 cycles (MPa)	4.86 ± 1.36	7.73 ± 1.94	7.55 ± 0.75	8.51 ± 0.73
Oxygen (wt%)	0.23	0.36	0.49	0.56
Nitrogen (wt%)	0.04	0.03	0.03	0.04
Hydrogen (wt%)	0.04	0.03	0.01	0.01

distinct from the shear bands seen for periodic lattices (where the same part of the unit cell fails simultaneously, leading to global shear band failure) and are likely to correspond to weak points of the stochastic

porous structure and planes where the resolved shear stress is maximised. Extensive cracking and fracture were observed at or near nodes between struts, while plastic deformation of struts was not observed. Fatigue testing revealed that all specimens exhibited similar fatigue failure behaviour with three distinct stages observed, regardless of the heat treatment condition (Fig. 3).

Plots of test stress against cycles to failure (S-N curves) for the four heat treatment conditions are seen in Fig. 4. The model used fits the data reasonably well in both the finite fatigue life and infinite fatigue life ranges. The as-built and 920 °C heat treatments show a greater spread of data than higher temperatures: ± 1.36 and ± 1.94 MPa respectively compared with ± 0.75 and ± 0.73 MPa for 1050 °C and 1200 °C heat treatments (note: these standard deviation values are shown in Table 1 for the σ_f at 10^6 cycles, but are valid for the entire S-N curve). Samples subjected to different heat treatments show similar behaviour in the finite fatigue life region of the S-N curve (decreasing stress region), however in the infinite fatigue life region (constant stress) there is significant difference between the samples, with as-built samples displaying lower fatigue strength than all others, with smaller variations between different heat treatment temperatures. The mean fatigue strength at 10^6 cycles was greatest for 1200 °C and 920 °C at 8.51 and 7.73 MPa respectively followed by 7.55 MPa for the 1050 °C specimens, with the as-built structures displaying the lowest fatigue strength at 4.86 MPa. The heat treatments investigated in this work result in an

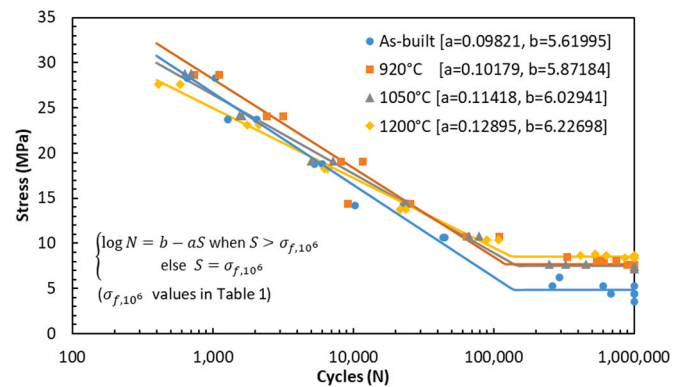


Fig. 4. S-N curves for compression fatigue testing of AM Ti64 stochastic lattices, in as-built condition and after vacuum heat treatment at 920, 1050, and 1200 °C. Data points at 10^6 cycles reached test end without failure during modified staircase method.

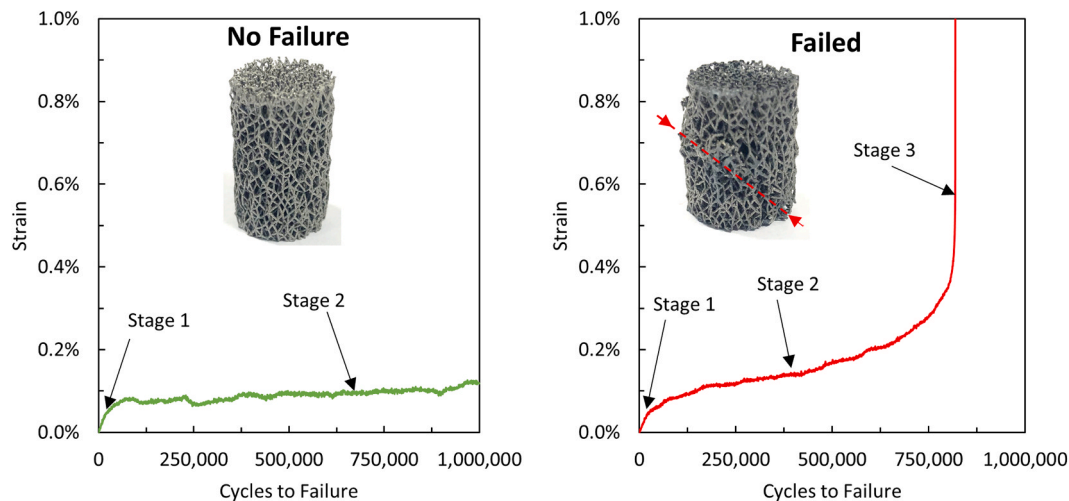


Fig. 3. Strain accumulation curves for AM Ti64 stochastic lattices during compressive fatigue testing, showing 10^6 cycles without failure (left) and with failure (right). Inset images show samples after testing.

increase in the high cycle fatigue behaviour of stochastic titanium porous structures by 55–75% compared to the as-built condition. The run-out for this study was set at one million cycles, however it does not appear that this is the endurance limit for titanium AM porous structures.

The Ti64 powder used in these experiments is specified to contain a maximum of 0.13 wt% O, 0.05 wt% N, and 0.012 wt% H [32], and elemental analysis of samples in as-built and heat treated conditions (Fig. 5) shows some deviation from this. For all samples the nitrogen content is comparable to what would be expected for the powder feedstock (0.03–0.04 wt%), indicating that the PBF process has not introduced additional nitrogen, and no changes are seen during heat treatment. The PBF process has clearly introduced some addition oxygen, and this continues with increasing heat treatment temperature, with the oxygen content going from 0.23 wt% in the as-built condition to 0.56 wt% for specimens heat treated at 1200 °C. The hydrogen content in the as-built condition is also higher at 0.04 wt% than the powder feedstock, however contrary to the oxygen content, as the heat treatment temperature increases the hydrogen content is reduced down to 0.01 wt%. This indicates that the vacuum heat treatment is effective at removing interstitial hydrogen in the alloy.

The morphological properties of the structure are summarised in Table 1. It would be expected that relative density and internal porosity would remain constant regardless of heat treatment. Variations are likely due to not scanning identical areas of the stochastic structure.

As the heat treatment temperature increases, the sintering neck size between semi-fused particles and struts increases, which can be observed in SEM images (Fig. 6). This reduces the variations in strut thickness, thereby reducing the outer diameter of the strut, which is consistent with micro-CT strut thickness measurements (Table 1). This also has the effect of increasing the core diameter of the strut [35], which is relevant for the mechanical properties.

Microstructural images for the various heat treatments are seen in Fig. 7, with light regions (α -phase) and the dark regions (β -phase) visible within individual struts. The microstructure of the as-built specimen is as expected: acicular α' -martensite. The acicular α' -grains are longer in the perpendicular direction, and there is also evidence of columnar prior β -grains. Gas entrapment pores are also observed within the struts of the as-built sample. These result from argon being trapped between build layers during the AM process, and can be identified by their characteristic spherical/elliptical shape, as opposed to lack of fusion pores, which have a more irregular shape [36]. After heat treatment at 920 °C a fine

lamellar microstructure is observed, along with some remaining anisotropy from the columnar prior β -grains, which has not been erased as the heat treatment is sub-transus. Small thin α -lathes are seen, with an increase in length in the perpendicular direction. Differences are seen when increasing the heat treatment temperature to above the β -transus. A coarse lamellar structure, with wide α -lathes is observed after heat treatment at both 1050 °C and 1200 °C. After these super-transus heat treatments there is little remaining anisotropy, with a similar extent of orientation of the α -lathes observed in the parallel direction and the perpendicular direction. Large α -lathes forming on prior β -grain boundaries were also seen after the 1200 °C heat treatment.

The inverse pole figures obtained by EBSD (Fig. 8) show evidence of columnar prior β -grains in both the as-built and 920 °C heat treated samples. After super-transus heat treatment all thermal history from the PBF fusion process is erased and there is no evidence of columnar prior β -grains. The EBSD images also show the thickening of the α' -martensite lathes from the as-built condition into lamellar α -grains after the 920 °C heat treatment. After super-transus (1050 and 1200 °C) heat treatment columnar prior β -grains cannot be seen, with these being replaced by large α colonies.

Solid specimens also produced by PBF underwent heat treatment simultaneously with their lattice counterparts to identify disparities in microstructure due to macro-morphology under identical processing conditions (Fig. 9). In the as-built condition both display a similar acicular α' -martensitic microstructure, with the porous specimen displaying slightly finer martensite. After heat treatment at 920 °C, the solid sample has a comparable fine lamellar microstructure to the porous specimen, with random orientation, however the α -lathes do appear slightly coarser. This trend is reversed for the super-transus heat treatments (1050 and 1200 °C), where the solid specimens show finer α -lathes than the porous specimens treated at the same temperature. These differences may be a result of the high surface area of the porous lattice, allowing variation in heat transfer behaviour compared with the solid samples. Both solid and porous specimens demonstrate increased orientation of the α -lathes after super-transus heat treatment, and the solid specimens show more evidence of α -lath formation along prior β -grain boundaries. The comparison between solid and porous structures indicates that microstructures can differ due to macro-morphology even under identical processing methods, emphasising the need to optimise heat treatment procedures depending on the fabrication method (conventional vs. AM) and geometry (solid vs. porous).

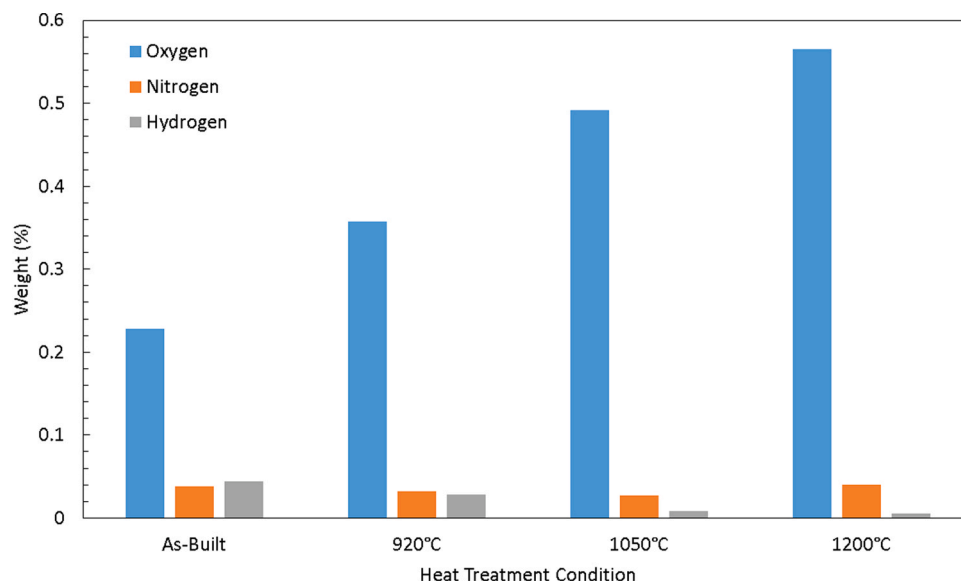


Fig. 5. LECO Elemental analysis results showing O, N and H content for samples in as-built condition and after vacuum heat treatment at 920, 1050, and 1200 °C.

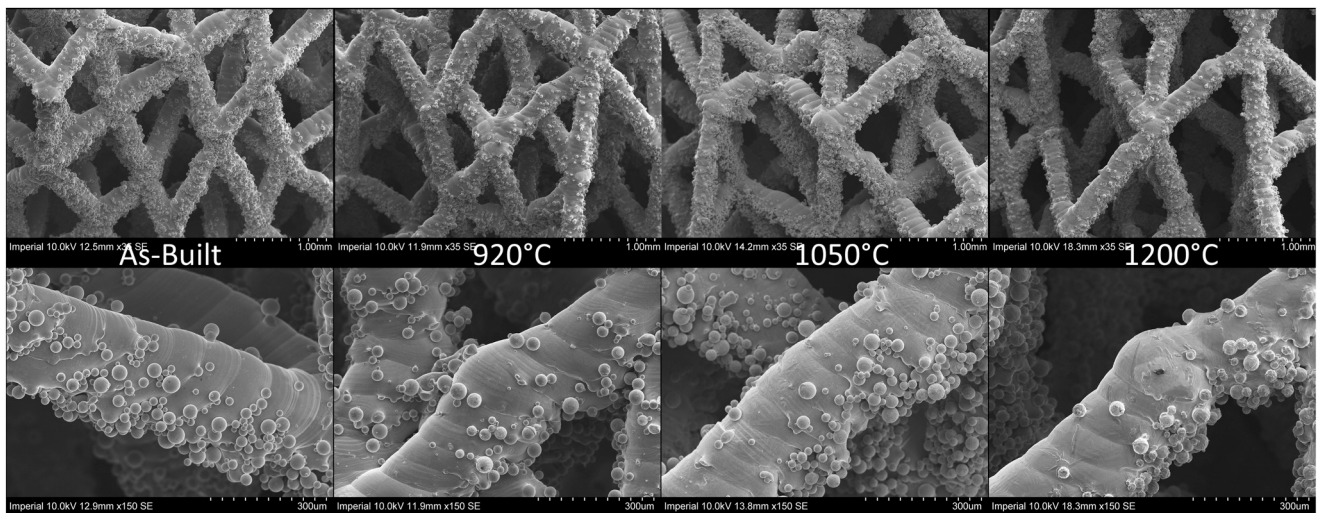


Fig. 6. SEM images showing the morphology of porous stochastic AM Ti64 lattices in as-built condition and after vacuum heat treatment at 920, 1050, and 1200 °C.

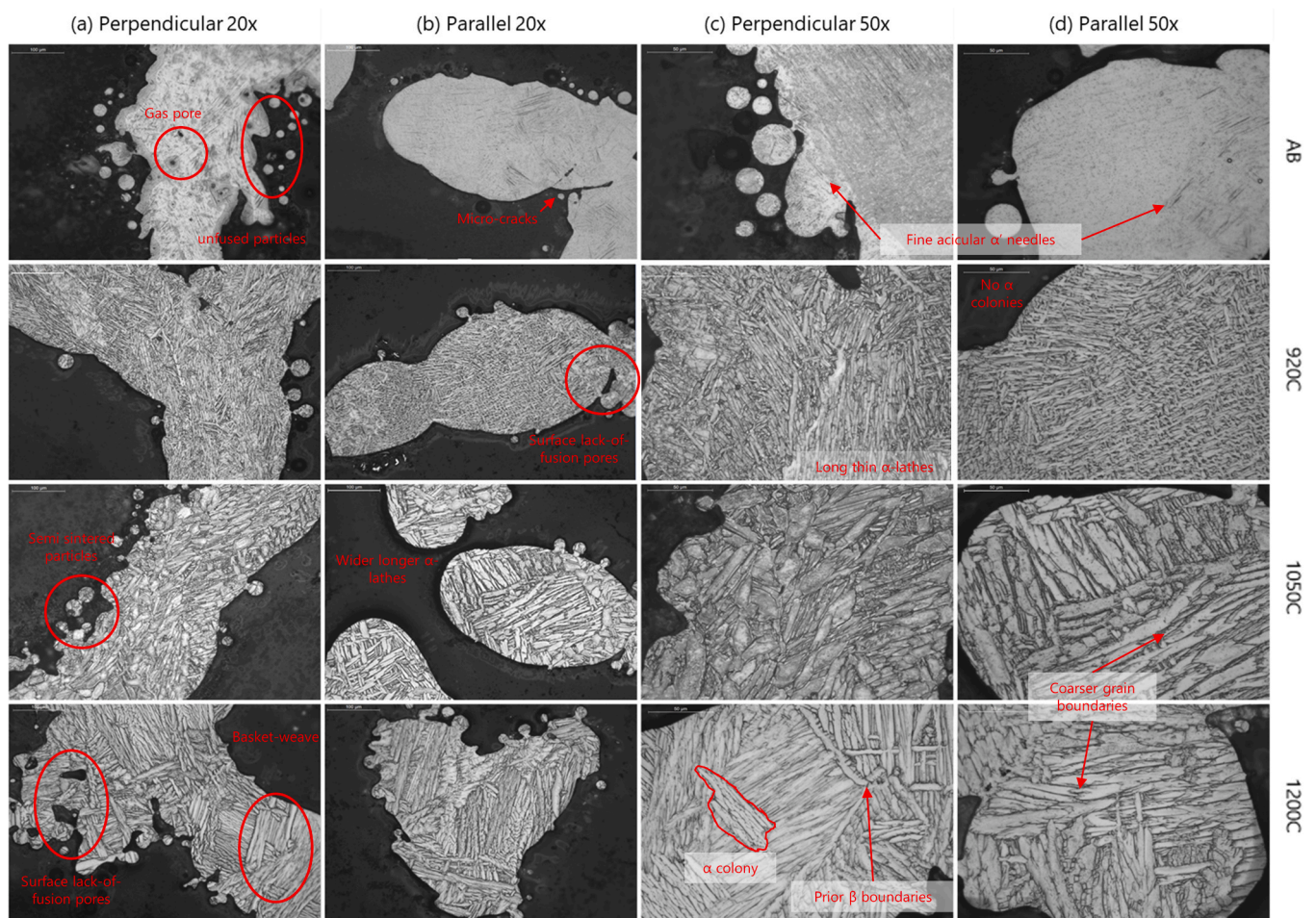


Fig. 7. Optical microscopy images showing the microstructures of AM Ti64 lattices in as-built condition and after vacuum heat treatment at 920, 1050, and 1200 °C. Samples were sectioned both perpendicular and parallel to the build direction, and images were taken at 20x and 50x magnification.

4. Discussion

By utilising sub-transus and super-transus vacuum heat treatment procedures, the microstructure of AM Ti64 porous lattices and their macro-scale strut morphology was modified, resulting in an increase in the compressive fatigue strength at 10^6 cycles of up to 75%. A range of

factors are responsible for these changes in properties including the elemental composition, heating and cooling rates, phase transformation, grain size and texture, which will be discussed further below.

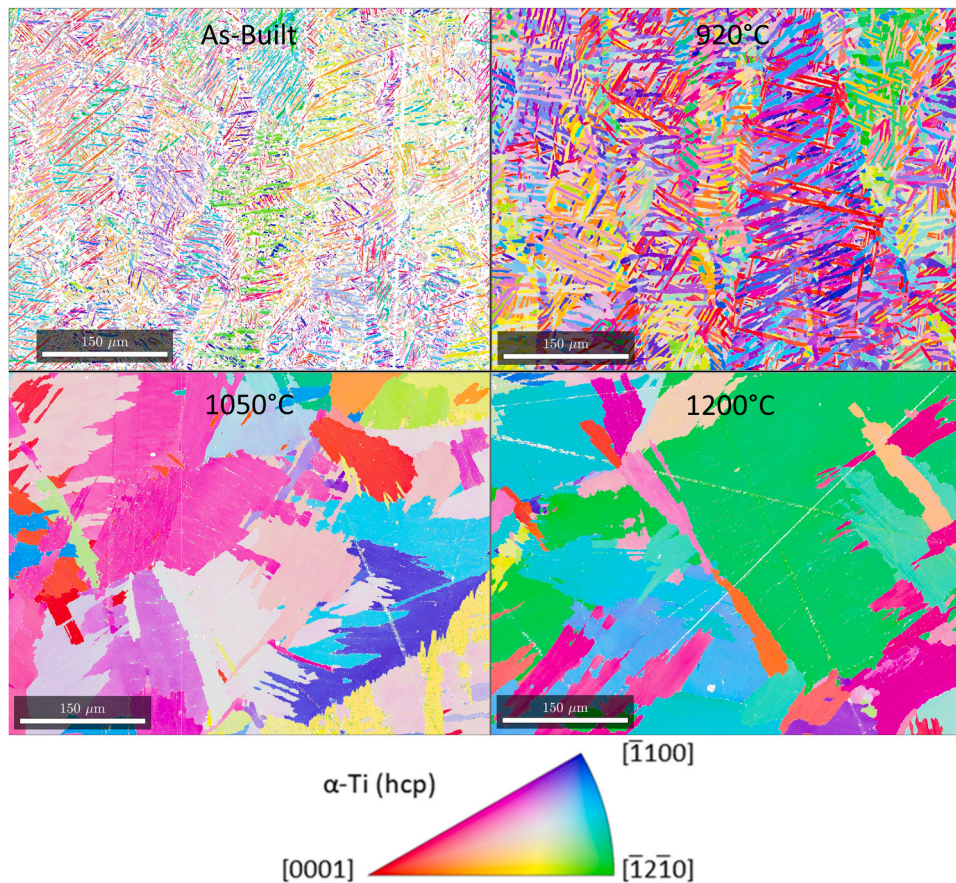


Fig. 8. EBSD inverse pole figure orientation maps showing microstructure evolution in AM Ti64 in as-built condition and after vacuum heat treatment at 920, 1050, and 1200 °C.

4.1. Composition

The variation in interstitial element composition for different heat treatment conditions has the potential to impact the mechanical properties. Oxygen pickup was found in the as-built and heat treated conditions due to the PBF and vacuum heat treatment processes, with higher heat treatment temperatures increasing oxygen pickup due to greater diffusivity. The oxygen content reached levels previously observed to cause increased strength and reduced ductility via solid solution hardening [37]. Hydrogen content has a similar but even greater effect on the mechanical properties relative to oxygen due to formation of hydrides, and although increased hydrogen content is seen in the as-built condition, vacuum heat treatment reduces this to less detrimental levels [26]. Although these changes might be expected to impact the measured mechanical properties, no variation in static yield strength was observed between different heat treatment conditions (Table 1), suggesting that the effects of changing O and H content are negligible or cancel each other out.

4.2. Microstructure

The microstructure observed in the as-built condition is consistent with previous work on AM Ti64 materials, where the fast cooling leads to a very fine martensitic microstructure [19–21,36,38]. It is well known that heat treatment of this fine martensitic structure displays different kinetics to Ti64 produced by conventional methods, and heat treatment procedures must be adjusted accordingly [22]. In this work, fine martensite is transformed to a fine lamellar microstructure after sub-transus heat treatment at 920 °C, while super-transus heat treatments at 1050 and 1200 °C result in coarse lamellar microstructures,

and anisotropy from directional solidification (i.e. columnar β -grains) is erased. This removal of as-built prior β -grain orientation after super-transus heat treatment, and formation of a coarser lamellar α microstructure is consistent with several previous studies on laser powder bed fusion of Ti64 [39–41]. Slight variations in the microstructure are also seen as a result of changes in the part geometry/macro-structure. Compared with the porous lattices, AM solid Ti64 has a coarser martensitic structure in the as-built condition, due to slower cooling during solidification. This is retained after sub-transus heat treatment (920 °C), with the fine lamellar structure being coarser than for the porous lattice after the same heat treatment. For super-transus heat treatments (1050, 1200 °C) the coarse lamellar microstructure is seen to be finer for the solid specimens compared with the porous lattices. The mechanism behind this difference is not clear but may be related to the slower heating and cooling rates in the solid specimens [42]. In other works these changes in heating and cooling rates have been shown to give rise to inhomogeneous microstructures within a single strut [43,44], however due to the smaller strut diameter used, and different alloy system, these effects are expected to be minor here. Optical micrographs of samples sectioned parallel to the build direction demonstrate this (Fig. 7), with no gradient microstructures observed. Due to their greater cross-sectional area, solid specimens also show a greater tendency for formation of α -laths along prior β -grain boundaries.

4.3. Static mechanical properties

The yield and maximum strength of the structures was relatively constant between the different heat treatment conditions ranging from ~32 to 35 MPa, while for comparison, maximally dense (after hot

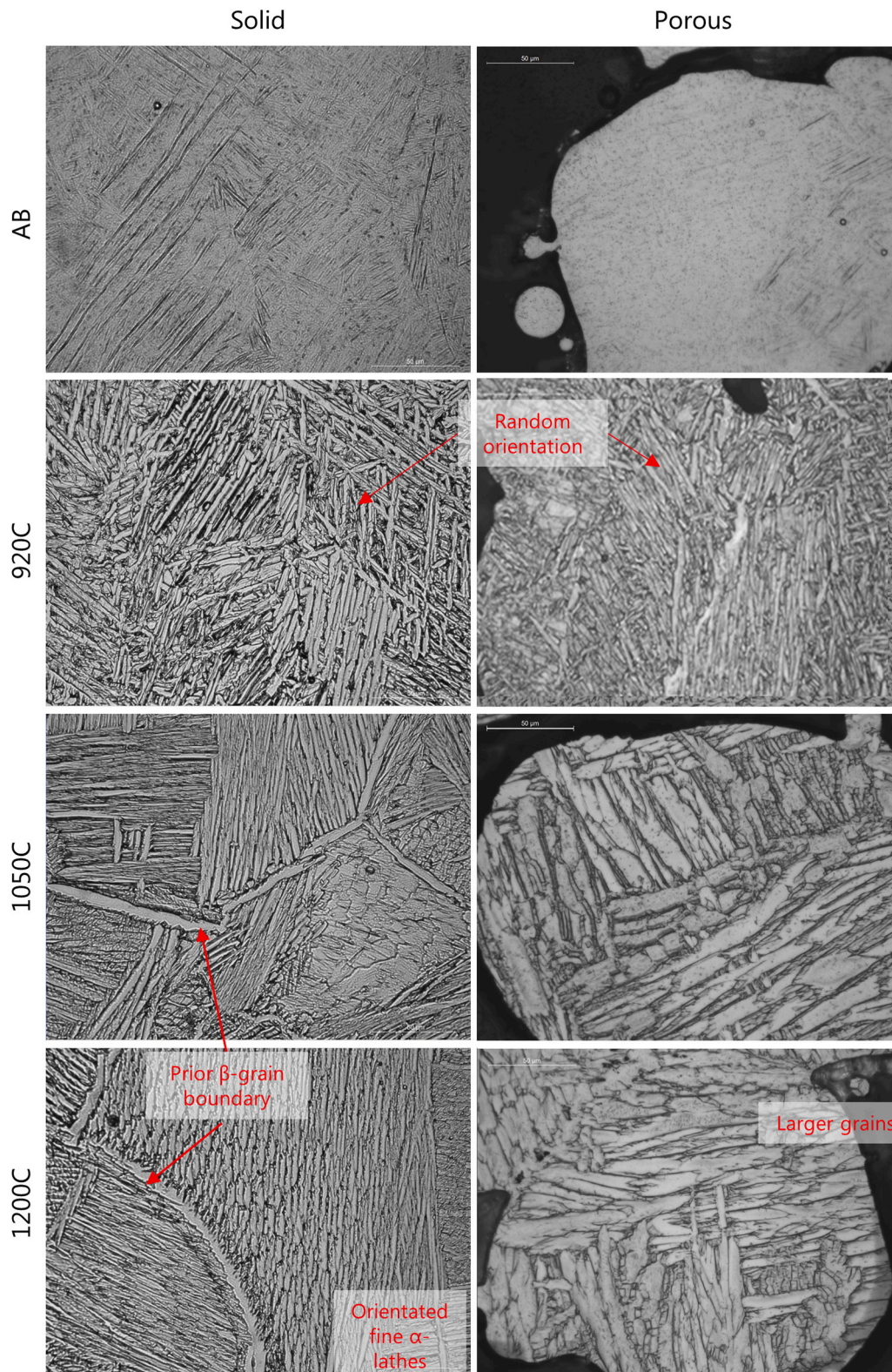


Fig. 9. Optical microscopy images showing the microstructures of AM Ti64 solid and porous lattice specimens in as-built condition and after vacuum heat treatment at 920, 1050, and 1200 °C. Samples sectioned parallel to the build direction, and images taken at 50x magnification.

isostatic pressing) additively manufactured specimens of this same material typically achieve a yield strength of 841 MPa [45]. The lower strengths observed here are a result of the high porosity (85–86%) and stress concentration and strut bending failure of the lattice structure. Previous work has also demonstrated that additively manufactured

Ti6Al4V micro-struts can display dramatically different properties compared with the bulk material, especially at low build angles, including reduced yield strength and elastic modulus [35,46,47].

The increase in the elastic modulus observed as the heat treatment temperature increases is interesting, as the elastic modulus of Ti64 does

not typically change significantly for different microstructures [48]. This behaviour can be explained as an effect of changes in the macro-scale morphology of the lattice structure. As observed from SEM images, sintering during higher heat treatment temperatures increases the neck size between semi-fused particles and struts, and also reduces the strut thickness variations that result from weld lines. These effects increase the minimum strut cross-section while keeping the average strut diameter relatively constant. Because the minimum strut cross-section is crucial for determining mechanical properties, this increase results in a corresponding increase in the elastic modulus.

An alternative explanation for the elastic modulus variation involves the loss of microstructural texture during heat treatment. During the AM process, it is well known that columnar β grains are formed, which are preferentially oriented with $\langle 001 \rangle_\beta$ directions parallel to the build direction [22,49,50]. The martensitic transformation occurs according to the Burgers orientation relationship $\{11\bar{0}\}_\beta || \langle 0001 \rangle_\alpha$, $\langle 001 \rangle_\beta || \langle 112\bar{0} \rangle_\alpha$, which means that the $\langle 0001 \rangle$ direction of the α' martensite or equilibrium α will be oriented at either 45° or 90° to the build direction $\langle 001 \rangle_\beta$ [51]. The hexagonal crystal structure introduces considerable mechanical anisotropy into the material (unlike the more isotropic bcc structure of the β phase), with single crystal α titanium known to have an elastic modulus of 145 GPa in the $\langle 0001 \rangle$ direction, but only 100 GPa perpendicular to this along the basal plane [48]. Therefore the as-built martensitic material will have its stiffest axis oriented 45° or 90° away from the build and test direction, reducing the measured modulus. After sub-transus heat treatment the anisotropy is reduced but is still evident in optical microscopy and EBSD. After super-transus heat treatment anisotropy from columnar β -grains is mostly erased, and the stiffer $\langle 0001 \rangle$ axis of the α -phase will be more randomly oriented, increasing the modulus when compared with the preferential off-axis orientation seen for as-built and sub-transus samples.

4.4. Dynamic mechanical properties

Due to the relatively high surface roughness, and extensive presence of semi-fused particles on the surface of the part, fatigue failure in AM Ti64 components is most often initiated by surface defects [52–54]. Although this can dominate the behaviour, microstructural effects still play a role in altering the crack propagation behaviour. The strong but brittle nature of the martensitic α' phase has poor resistance to crack propagation [20], leading to the low fatigue strength seen here for the as-built porous Ti64 lattices. The presence of gas entrapment pores in the as-built sample is also likely to play a role in reducing the fatigue life, as these can act as internal crack initiation sites [55]. Gas entrapment pores were not observed in microscopy images of samples after heat treatment, suggesting that both sub-transus and super-transus vacuum heat treatment was sufficient to remove these pores. Despite this, differences in internal porosity were not detected by μ CT, although this could be an effect of the μ CT resolution ($5\ \mu\text{m}$) being insufficient to detect these small pores. After sub-transus heat treatment at 920°C , the α' martensite is transformed to fine lamellar $\alpha + \beta$. Here the presence of the β -phase (which is less favourable for crack propagation), as well as the high density of α/β phase boundaries, makes crack propagation more difficult [21] and therefore increases the fatigue strength. Super-transus heat treatments at 1050 and 1200°C also result in lamellar $\alpha + \beta$ microstructures, however these have a much coarser structure with wider and longer α -laths. Previous work has shown that increasing the α -lath width significantly reduces the fatigue strength, due to faster crack propagation through the α -phase [11,12,56]. This explains the reduced fatigue strength observed for the samples heat treated at 1050°C , compared with the fatigue strength achieved after 920°C heat treatment – the greatly increased α -lath size reduces the resistance of the microstructure to crack propagation. The porous lattices samples heat treated at 1200°C have a similar coarse lamellar microstructure, however these display the highest fatigue strength of all the conditions tested at 8.62 MPa (after 10^6 cycles). This is unlikely to be caused by a change in

the microstructure, as the microstructures of porous samples heat treated at 1050 and 1200°C are quite similar in morphology and scale. Changes in the macro-scale morphology (i.e. the porous lattice structure) are a more likely explanation for these differences in fatigue strength. SEM images indicate that higher heat treatment temperatures increase the neck size where semi-fused particles are joined to struts, as well as reducing thickness variations. This has the effect of reducing the defect size on the surface of the struts, which has been shown to have a dramatic effect on the fatigue strength of AM Ti64 [17,57,58]. The effect of surface defects is even more pronounced here due to the porous nature of the fatigue specimens, as their surface area to volume ratio is higher than bulk AM parts, therefore even slight reductions in initial crack size can have a considerable effect on the overall fatigue properties.

Our finding that super-transus heat treatment provides superior fatigue strength to sub-transus heat treatment somewhat contradicts findings by Kumar et al. on PBF Ti64, who observed that the α/β basketweave microstructure formed sub-transus provides enhanced resistance to fatigue crack growth, while the coarser microstructure formed super-transus offers less resistance [41]. These tests were carried out on additively manufactured solid samples however, further emphasising the distinct behaviour of lattice materials, where changes in strut morphology can have a large effect. On lattice materials, Ahmadi et al. conducted a range of post-processing treatments including sub-transus (800°C) and super-transus (1050°C) heat treatments, finding similar changes in microstructure (fine lamellar at 800°C , coarse lamellar at 1050°C), and fatigue strength increasing in the order as-built, sub-transus treatment, and super-transus treatment [59]. The size of this effect was small however, which may be associated with the use of an argon furnace atmosphere rather than vacuum. Brenne et al. conducted vacuum heat treatment of AM Ti64 cellular structures, confirming the results seen here that super-transus heat treatment leads to coarsening of the lamellar microstructure and improved fatigue behaviour, although full S-N testing and sub-transus heat treatment were not carried out [27].

4.5. Limitations

Despite the findings discussed above, this study does have some limitations that can affect the ability to draw definitive conclusions from these results. An unavoidable consequence of the vacuum heat treatment procedure is the fact that multiple different properties of the samples are altered simultaneously. This includes elemental composition, grain texture, and strut morphology. As a result it can be challenging to separate the effects of different phenomena on the resulting mechanical properties. This could be addressed in future work by conducting similar investigations on samples with varying build orientations, to separate the effect of grain texture from the PBF solidification process. Our study investigated the effect of heat treatments on the fatigue strength, but other parameters such as machine process parameters and lattice design have been shown to affect the modulus, yield strength and fatigue strength of lattice structures. Therefore, while reporting on heat treatments is useful, if the goal is to maximise fatigue life these other variables must also be considered. In addition, although the data presented here allow differences in the fatigue strength of porous AM Ti64 for different heat treatment conditions to be observed and explained, the sample size used here is sufficient only for exploratory S-N testing and not full reliability assessment [34]. Further research using a larger sample size ($n \geq 30$) would allow S-N curves to be used for design and reliability purposes.

5. Conclusions

The results presented here demonstrated that coarse and fine lamellar microstructures comparable to those seen in conventional wrought Ti64 can also be achieved in porous AM Ti64, through the use

of vacuum heat treatment. These heat treatment procedures require optimisation for different processing routes and sample geometries; here fine lamellar microstructures were achieved using 2 h sub-transus heat treatment at 920 °C followed by furnace cooling, while coarse lamellar microstructures were achieved using 2 h super-transus heat treatment at 1050 °C or 1200 °C, followed by furnace cooling.

The static yield strength of porous AM Ti64 did not change for different heat treatment conditions, however the elastic modulus showed a consistent increase with increasing heat treatment temperature, increasing from 2552 ± 22 MPa for as-built samples to 2968 ± 45 MPa after heat treatment at 1200 °C. This can be understood as a combination of strut sintering increasing the effective strut thickness, and/or removal of the prior columnar β -grain texture which orients the strongest axis of the α -phase away from the loading axis.

Increases in the fatigue strength of porous AM Ti64 were achieved after heat treatment. Sub-transus heat treatment eliminated the brittle α' martensite phase in favour of a fine $\alpha + \beta$ mixture, where the high density of phase boundaries and β content provides high resistance to crack propagation. Super-transus heat treatments increased the α -lath size which has a detrimental effect on crack propagation resistance, however strut sintering effects are thought to have reduced surface crack initiation sites, leading to a maximum fatigue strength (at 10^6 cycles) of 8.51 ± 0.73 MPa, an increase of 75% from the fatigue strength of the as-built material of 4.86 ± 1.36 MPa.

CRediT authorship contribution statement

Shaaz Ghouse: Conceptualization, Methodology, Investigation, Resources, Validation, Writing – Original Draft, Review & Editing, Visualization. **Reece N. Oosterbeek:** Formal analysis, Writing – Original Draft, Review & Editing, Visualization. **Aisha Tayub Mehmood:** Methodology, Investigation, Visualization. **Filippo Vecchiato:** Investigation, Supervision. **Jonathan R.T. Jeffers:** Conceptualization, Supervision, Funding acquisition, Project administration, Writing – Review & Editing.

Declaration of Competing Interest

The authors declare that they have no known competing financial interests or personal relationships that could have appeared to influence the work reported in this paper.

Acknowledgements

The authors wish to gratefully acknowledge support from the Engineering and Physical Sciences Research Council (EP/R042721/1), Wellcome Trust (208858/Z/17/Z), and National Institute for Health Research (NIHR300013).

References

- [1] A.A. Shapero, J.P. Borgonia, Q.N. Chen, R.P. Dillon, B. McEnerney, R. Polit-Casillas, L. Soloway, Additive manufacturing for aerospace flight applications, *J. Spacecr. Rockets* 53 (5) (2016) 952–959, <https://doi.org/10.2514/1.A33544>.
- [2] J. Plocher, A. Panesar, Review on design and structural optimisation in additive manufacturing: towards next-generation lightweight structures, *Mater. Des.* 183 (2019), 108164, <https://doi.org/10.1016/j.matdes.2019.108164>.
- [3] C. Emmelmann, P. Sander, J. Kranz, E. Wycisk, Laser additive manufacturing and bionics: redefining lightweight design, *Phys. Procedia* 12 (PART 1) (2011) 364–368, <https://doi.org/10.1016/j.phpro.2011.03.046>.
- [4] Y.L. Hao, S.J. Li, R. Yang, Biomedical titanium alloys and their additive manufacturing, *Rare Metals* 35 (9) (2016) 661–671, <https://doi.org/10.1007/s12598-016-0793-5>.
- [5] S. Ghouse, N. Reznikov, O.R. Boughton, S. Babu, K.C.G. Ng, G. Blunn, J.P. Cobb, M. M. Stevens, J.R.T. Jeffers, The design and in vivo testing of a locally stiffness-matched porous scaffold, *Appl. Mater. Today* 15 (2019) 377–388, <https://doi.org/10.1016/j.apmt.2019.02.017>.
- [6] X.Y. Zhang, G. Fang, S. Leeftang, A.A. Zadpoor, J. Zhou, Topological design, permeability and mechanical behavior of additively manufactured functionally graded porous metallic biomaterials, *Acta Biomater.* 84 (2019) 437–452, <https://doi.org/10.1016/j.actbio.2018.12.013>.
- [7] X. Wang, S. Xu, S. Zhou, W. Xu, M. Leary, P. Choong, M. Qian, M. Brandt, Y.M. Xie, Topological design and additive manufacturing of porous metals for bone scaffolds and orthopaedic implants: a review, *Biomaterials* 83 (2016) 127–141, <https://doi.org/10.1016/j.biomaterials.2016.01.012>.
- [8] S. Amin Yavari, R. Wauthle, J. Van Der Stok, A.C. Riemsdijk, M. Janssen, M. Mulier, J.P. Kruth, J. Schrooten, H. Weinans, A.A. Zadpoor, Fatigue behavior of porous biomaterials manufactured using selective laser melting, *Mater. Sci. Eng. C* 33 (8) (2013) 4849–4858, <https://doi.org/10.1016/j.msec.2013.08.006>.
- [9] S.M. Ahmadi, R. Hedayati, Y. Li, K. Lietaert, N. Tümer, A. Fatemi, C.D. Rans, B. Pouran, H. Weinans, A.A. Zadpoor, Fatigue performance of additively manufactured meta-biomaterials: the effects of topology and material type, *Acta Biomater.* 65 (2018) 292–304, <https://doi.org/10.1016/j.actbio.2017.11.014>.
- [10] G.Q. Wu, C.L. Shi, W. Sha, A.X. Sha, H.R. Jiang, Effect of microstructure on the fatigue properties of Ti-6Al-4V titanium alloys, *Mater. Des.* 46 (2013) 668–674, <https://doi.org/10.1016/j.matdes.2012.10.059>.
- [11] Y. Fan, W. Tian, Y. Guo, Z. Sun, J. Xu, Relationships among the microstructure, mechanical properties, and fatigue behavior in thin Ti6Al4V, *Adv. Mater. Sci. Eng.* 2016 (2016), <https://doi.org/10.1155/2016/7278267>.
- [12] G. Lutjering, A. Gysler, “Fatigue: a Critical Review,” in *Titanium ’84: Science and Technology*, Proc. 5th World Conference on Titanium, Munich, Germany, September 1984, 1984, pp. 2065–2083.
- [13] R.K. Nalla, B.L. Boyce, J.P. Campbell, J.O. Peters, R.O. Ritchie, Influence of microstructure on high-cycle fatigue of Ti-6Al-4V: bimodal vs. lamellar structures, *Metall. Mater. Trans. A Phys. Metall. Mater. Sci.* 33 (A) (2002) 899–918.
- [14] J.O. Peters, G. Lutjering, Comparison of the fatigue and fracture of $\alpha + \beta$ and β titanium alloys, *Metall. Mater. Trans. A* 32 (2001) 2805–2818.
- [15] J.H. Zuo, Z.G. Wang, E.H. Han, Effect of microstructure on ultra-high cycle fatigue behavior of Ti-6Al-4V, *Mater. Sci. Eng. A* 473 (1–2) (2008) 147–152, <https://doi.org/10.1016/j.msea.2007.04.062>.
- [16] S. Bagehorn, J. Wehr, H.J. Maier, Application of mechanical surface finishing processes for roughness reduction and fatigue improvement of additively manufactured Ti-6Al-4V parts, *Int. J. Fatigue* 102 (2017) 135–142, <https://doi.org/10.1016/j.ijfatigue.2017.05.008>.
- [17] E. Wycisk, C. Emmelmann, S. Siddique, F. Walther, High cycle fatigue (HCF) performance of Ti-6Al-4V alloy processed by selective laser melting, *Adv. Mater. Res.* 816–817 (2013) 134–139, <https://doi.org/10.4028/www.scientific.net/AMR.816-817.134>.
- [18] W. Hansal, S. Hansal, G. Sandalachie, “US PATENT US 2020/0080222 A1: ELECTROPOLISHING METHOD AND ELECTROLYTE FOR SAME,” US 2020/0080222 A1, 2020.
- [19] P. Li, D.H. Warner, A. Fatemi, N. Phan, Critical assessment of the fatigue performance of additively manufactured Ti-6Al-4V and perspective for future research, *Int. J. Fatigue* 85 (2016) 130–143, <https://doi.org/10.1016/j.ijfatigue.2015.12.003>.
- [20] W. Xu, S. Sun, J. Elambasseril, Q. Liu, M. Brandt, M. Qian, Ti-6Al-4V additively manufactured by selective laser melting with superior mechanical properties, *JOM J. Miner. Metals Mater. Soc.* 67 (3) (2015) 668–673, <https://doi.org/10.1007/s11837-015-1297-8>.
- [21] Y. Zhai, H. Galarraga, D.A. Lados, Microstructure, static properties, and fatigue crack growth mechanisms in Ti-6Al-4V fabricated by additive manufacturing: LENS and EBM, *Eng. Fail. Anal.* 69 (2016) 3–14, <https://doi.org/10.1016/j.engfailanal.2016.05.036>.
- [22] B. Vrancken, L. Thijs, J.P. Kruth, J. Van Humbeeck, Heat treatment of Ti6Al4V produced by Selective Laser Melting: microstructure and mechanical properties, *J. Alloy. Compd.* 541 (2012) 177–185, <https://doi.org/10.1016/j.jallcom.2012.07.022>.
- [23] E. Brandl, D. Greitemeier, Microstructure of additive layer manufactured Ti-6Al-4V after exceptional post heat treatments, *Mater. Lett.* 81 (2012) 84–87, <https://doi.org/10.1016/j.matlet.2012.04.116>.
- [24] X. Li, J. Xie, Y. Zhou, Effects of oxygen contamination in the argon shielding gas in laser welding of commercially pure titanium thin sheet, *J. Mater. Sci.* 40 (13) (2005) 3437–3443, <https://doi.org/10.1007/s10853-005-0447-8>.
- [25] F.H. Froes, *Titanium: Physical Metallurgy Processing and Application*, ASM International, Materials Park, OH, 2015.
- [26] M.J. Donachie, *Titanium a Technical Guide*, 2nd ed., ASM International, Materials Park, OH, 2000.
- [27] F. Brenne, T. Niendorf, H.J. Maier, Additively manufactured cellular structures: impact of microstructure and local strains on the monotonic and cyclic behavior under uniaxial and bending load, *J. Mater. Process. Technol.* 213 (9) (2013) 1558–1564, <https://doi.org/10.1016/j.jmatprotec.2013.03.013>.
- [28] R. Wauthle, B. Vrancken, B. Beynaerts, K. Jorissen, J. Schrooten, J.P. Kruth, J. Van Humbeeck, Effects of build orientation and heat treatment on the microstructure and mechanical properties of selective laser melted Ti6Al4V lattice structures, *Addit. Manuf.* 5 (2015) 77–84, <https://doi.org/10.1016/j.addma.2014.12.008>.
- [29] S. Ghouse, S. Babu, R.J. Van Arkel, K. Nai, P.A. Hooper, J.R.T. Jeffers, The influence of laser parameters and scanning strategies on the mechanical properties of a stochastic porous material, *Mater. Des.* 131 (2017) 498–508, <https://doi.org/10.1016/j.matdes.2017.06.041>.
- [30] S. Ghouse, S. Babu, K. Nai, P.A. Hooper, J.R.T. Jeffers, The influence of laser parameters, scanning strategies and material on the fatigue strength of a stochastic porous structure, *Addit. Manuf.* 22 (2018) 290–301, <https://doi.org/10.1016/j.addma.2018.05.024>.

- [31] British Standards Institution, BS ISO 13314:2011 Mechanical testing of metals, ductility testing, compression test for porous and cellular metals, BSI Standards Limited, 2011.
- [32] ASTM, ASTM F3001-14: Standard Specification for Additive Manufacturing Titanium-6 Aluminum-4 Vanadium ELI (Extra Low Interstitial) with Powder Bed Fusion, Annu. B. ASTM Stand., 2014, doi: 10.1520/F3001-14.
- [33] British Standards Institution, BS ISO 1099:2017 Metallic materials — Fatigue Testing — Axial Force-controlled Method, BSI Standards Limited, 2017.
- [34] International Organization for Standardization, ISO 12107:2003 Metallic materials — Fatigue testing — Statistical planning and analysis of data, 2003.
- [35] U. Hossain, S. Ghouse, K. Nai, J. Jeffers, Mechanical and morphological properties of additively manufactured SS316L and Ti6Al4V micro-struts as a function of build angle, *Addit. Manuf.* 46 (2021), 102050, <https://doi.org/10.1016/j.addma.2021.102050>.
- [36] S. Liu, Y.C. Shin, Additive manufacturing of Ti6Al4V alloy: a review, *Mater. Des.* 164 (2019), 107552, <https://doi.org/10.1016/j.matdes.2018.107552>.
- [37] Z. Liu, G. Welsch, Effects of oxygen and heat treatment on the mechanical properties of alpha and beta titanium alloys, *Metall. Trans. A* 19 (3) (1988) 527–542, <https://doi.org/10.1007/BF02649267>.
- [38] J. Yang, H. Yu, J. Yin, M. Gao, Z. Wang, X. Zeng, Formation and control of martensite in Ti-6Al-4V alloy produced by selective laser melting, *Mater. Des.* 108 (2016) 308–318, <https://doi.org/10.1016/j.matdes.2016.06.117>.
- [39] T. Vilaro, C. Colin, J.D. Bartout, As-fabricated and heat-treated microstructures of the Ti-6Al-4V alloy processed by selective laser melting, *Metall. Mater. Trans. A Phys. Metall. Mater. Sci.* 42 (10) (2011) 3190–3199, <https://doi.org/10.1007/s11661-011-0731-y>.
- [40] S.Q. Wu, Y.J. Lu, Y.L. Gan, T.T. Huang, C.Q. Zhao, J.J. Lin, S. Guo, J.X. Lin, Microstructural evolution and microhardness of a selective-laser-melted Ti-6Al-4V alloy after post heat treatments, *J. Alloy. Compd.* 672 (2016) 643–652, <https://doi.org/10.1016/j.jallcom.2016.02.183>.
- [41] P. Kumar, U. Ramamurthy, Microstructural optimization through heat treatment for enhancing the fracture toughness and fatigue crack growth resistance of selective laser melted Ti-6Al-4V alloy, *Acta Mater.* 169 (2019) 45–59, <https://doi.org/10.1016/j.actamat.2019.03.003>.
- [42] L.E. Murr, S.M. Gaytan, F. Medina, E. Martinez, J.L. Martinez, D.H. Hernandez, B. I. Machado, D.A. Ramirez, R.B. Wicker, Characterization of Ti-6Al-4V open cellular foams fabricated by additive manufacturing using electron beam melting, *Mater. Sci. Eng. A* 527 (7–8) (2010) 1861–1868, <https://doi.org/10.1016/j.msea.2009.11.015>.
- [43] M. Liu, N. Takata, A. Suzuki, M. Kobashi, Development of gradient microstructure in the lattice structure of AlSi10Mg alloy fabricated by selective laser melting, *J. Mater. Sci. Technol.* 36 (2020) 106–117, <https://doi.org/10.1016/j.jmst.2019.06.015>.
- [44] M. Liu, N. Takata, A. Suzuki, M. Kobashi, Effect of heat treatment on gradient microstructure of AlSi10Mg lattice structure manufactured by laser powder bed fusion, *Materials* 13 (11) (2020) 2487, <https://doi.org/10.3390/ma13112487>.
- [45] Carpenter Additive, “PowderRange Ti64 datasheet,” 2020. (<https://www.carpenteradditive.com/powderrange-powders>) (accessed 21 June 2021).
- [46] Z. Wang, P. Li, Characterisation and constitutive model of tensile properties of selective laser melted Ti-6Al-4V struts for microlattice structures, *Mater. Sci. Eng. A* 725 (2018) 350–358, <https://doi.org/10.1016/j.msea.2018.04.006>.
- [47] R. Hasan, A.W. Mines, S. Tsopanos, R.A.W. Mines, S. Tsopanos, Determination of elastic modulus value for selectively laser melted titanium alloy, *J. Mech. Eng. Technol.* 2 (2) (2010) 17–26.
- [48] C. Leyens, M. Peters, Titanium and Titanium Alloys: Fundamentals and Applications, Wiley-VCH, Chichester, 2003.
- [49] L. Thijs, F. Verhaeghe, T. Craeghs, J. Van Humbeeck, J.P. Kruth, A study of the microstructural evolution during selective laser melting of Ti-6Al-4V, *Acta Mater.* 58 (9) (2010) 3303–3312, <https://doi.org/10.1016/j.actamat.2010.02.004>.
- [50] P.A. Kobryn, S.L. Semiatin, Microstructure and texture evolution during solidification processing of Ti-6Al-4V, *J. Mater. Process. Technol.* 135 (2003) 330–339, [https://doi.org/10.1016/S0924-0136\(02\)00865-8](https://doi.org/10.1016/S0924-0136(02)00865-8).
- [51] X. Shui, K. Yamanaka, M. Mori, Y. Nagata, K. Kurita, A. Chiba, Effects of post-processing on cyclic fatigue response of a titanium alloy additively manufactured by electron beam melting, *Mater. Sci. Eng. A* 680 (2017) 239–248, <https://doi.org/10.1016/j.msea.2016.10.059>.
- [52] V. Chastand, P. Quaegebeur, W. Maia, E. Charkaluk, Comparative study of fatigue properties of Ti-6Al-4V specimens built by electron beam melting (EBM) and selective laser melting (SLM), *Mater. Charact.* 143 (2018) 76–81, <https://doi.org/10.1016/j.matchar.2018.03.028>.
- [53] A.W. Prabhu, T. Vincent, A. Chaudhary, W. Zhang, S.S. Babu, Effect of microstructure and defects on fatigue behaviour of directed energy deposited Ti-6Al-4V, *Sci. Technol. Weld. Join.* 20 (8) (2015) 659–669, <https://doi.org/10.1179/1362171815Y.0000000050>.
- [54] E. Wycisk, A. Solbach, S. Siddique, D. Herzog, F. Walther, C. Emmelmann, Effects of defects in laser additive manufactured Ti-6Al-4V on fatigue properties, *Phys. Procedia* 56 (C) (2014) 371–378, <https://doi.org/10.1016/j.phpro.2014.08.120>.
- [55] S. Leuders, M. Thöne, A. Riemer, T. Niendorf, T. Tröster, H.A. Richard, H.J. Maier, On the mechanical behaviour of titanium alloy TiAl6V4 manufactured by selective laser melting: fatigue resistance and crack growth performance, *Int. J. Fatigue* 48 (2013) 300–307, <https://doi.org/10.1016/j.ijfatigue.2012.11.011>.
- [56] M. Hassanipour, S. Watanabe, K. Hirayama, H. Toda, K. Uesugi, A. Takeuchi, Short crack growth behavior and its transitional interaction with 3D microstructure in Ti-6Al-4V, *Mater. Sci. Eng. A* 738 (2018) 229–237, <https://doi.org/10.1016/j.msea.2018.09.073>.
- [57] S. Tammis-Williams, P.J. Withers, I. Todd, P.B. Prangnell, The influence of porosity on fatigue crack initiation in additively manufactured titanium components, *Sci. Rep.* 7 (1) (2017) 1–13, <https://doi.org/10.1038/s41598-017-06504-5>.
- [58] D. Greitemeier, C. Dalle Donne, F. Syassen, J. Eufinger, T. Melz, Effect of surface roughness on fatigue performance of additive manufactured Ti-6Al-4V, *Mater. Sci. Technol.* 32 (7) (2016) 629–634, <https://doi.org/10.1179/1743284715Y.0000000053>.
- [59] S.M. Ahmadi, R. Kumar, E.V. Borisov, R. Petrov, S. Leeflang, Y. Li, N. Tümer, R. Huizenga, C. Ayas, A.A. Zadpoor, V.A. Popovich, From microstructural design to surface engineering: a tailored approach for improving fatigue life of additively manufactured meta-biomaterials, *Acta Biomater.* 83 (2019) 153–166, <https://doi.org/10.1016/j.actbio.2018.10.043>.